Obrabotka metallov (tekhnologiya, oborudovanie, instrumenty) = Metal Working and Material Science. 2022 vol. 24 no. 4 pp. 219–242
ISSN: 1994-6309 (print) / 2541-819X (online)
DOI: 10.17212/1994-6309-2022-24.4-219-242

NSTU NETI

Obrabotka metallov -
Metal Working and Material Science

Journal homepage: http://journals.nstu.ru/obrabotka_metallov

The study of characteristics of the structure of metallic alloys using synchrotron radiation computed laminography (Research Review)

Oleg Kutkin [1, a, *], *Ivan Bataev* [1, b], *Gleb Dovzhenko* [2, c], *Zinaida Bataeva*[3, d]

[1] Novosibirsk State Technical University, 20 Prospekt K. Marksa, Novosibirsk, 630073, Russian Federation
[2] Siberian Circular Photon Source "SKlF" Boreskov Institute of Catalysis of Siberian Branch of the Russian Academy of Sciences (SRF "SKIF"), 1 Nikol'skii pr., Kol'tsovo, 630559, Russian Federation
[3] Siberian State University of water transport, 33 Schetinkina str., Novosibirsk, 630099, Russian Federation

[a] https://orcid.org/0000-0003-1277-388X, kutkino@list.ru, [b] https://orcid.org/0000-0003-2871-0269, i.bataev@corp.nstu.ru,
[c] https://orcid.org/0000-0003-0615-0643, g.dovjenko@skif.ru [d] https://orcid.org/0000-0001-5027-6193, bataevazb@ngs.ru

ARTICLE INFO

Article history:
Received: 04 October 2022
Revised: 02 November 2022
Accepted: 03 November 2022
Available online: 15 December 2022

Keywords:
Computed tomography
Computed laminography
X-ray visualization methods
Synchrotron radiation

Funding
This research was funded by the Federal Task of Ministry of Education and Science of the Russian Federation (project FSUN-2020-0014 (2019-0931): "Investigations of Metastable Structures Formed on Material Surfaces and Interfaces under Extreme External Impacts".

ABSTRACT

The paper contains a review of research related to the use of synchrotron radiation computed laminography in the study of the structure features of metal alloys subjected to various methods of external action. **Introduction**. The important role of X-rays in the field of materials research is discussed. The capabilities of standard X-ray devices equipped with X-ray tubes and modern synchrotron radiation (*SR*) sources with unique parameters are compared. **Methods for studying flat samples. Tomography and synchrotron laminography**. An informative method based on the use of synchrotron X-rays is synchrotron radiation computed tomography (*SRCT*), which allows obtaining cross-section images of objects by processing multiple absorption radiographs. A brief classification of five generations of tomographs is presented. The problems encountered in obtaining data from non-compact (non-isometric) samples are avoided by using the method of synchrotron radiation computed laminography (*SRCL*), which combines the principles of laminography with the advantages of synchrotron imaging. Currently the method is used for non-destructive testing of non-isometric objects by a number of synchrotron radiation sources (*ESRF*, *ANKA*, *Spring-8*). **Resolution of synchrotron radiation computed laminography**. The use of monochromatic radiation in realization of computed laminography method is a factor, which provides high spatial resolution down to micron and submicron scale. An equally important factor is related to the characteristics of the detector. Images with a resolution of ~100 nm were obtained using nanolaminography**. Comparison of laminography and tomography methods. Augmented laminography**. *Augmented laminography* allows improving image quality by augmenting the Fourier space analyzed by laminography with information obtained from lower resolution *CT*. Reconstruction performed using *Augmented laminography* is characterized by the absence of significant artifacts and high resolution. **Implementation of the laminography method**. The angle of inclination of the rotary axis θ (*SRCL* method) is related to the geometry of samples and is determined experimentally in each case. In order to achieve the necessary resolution, the value θ should provide an optimal average value of the intensity of the passed radiation. The energy of X-rays is calculated on the basis of material characteristics. To reconstruct images of the objects, software complexes that implement the filtered back projection method based on the Radon transform are used. **Examples of laminography application for analysis of metal alloys samples**. The laminography method can be used for in-situ investigations allowing real time monitoring of processes occurring under different conditions of external action, e.g. during plastic deformation of metal plates. Data on formation of pore-type defects in the process of loading of metal workpieces are interesting. Numerous examples of post-mortem studies of metal alloys for various purposes are described in the literature. Important information is obtained in the study of fatigue cracks, as well as defects arising in the process of contact-fatigue loading of materials. **Conclusion**. The *SRCT* and *SRCL* methods are rationally implemented at the generation 4+ synchrotron radiation source "*SKIF*" under construction in Novosibirsk.

For citation: Kutkin O.M., Bataev I.A., Dovzhenko G.D., Bataeva Z.B. The study of characteristics of the structure of metallic alloys using synchrotron radiation computed laminography (Research Review). *Obrabotka metallov (tekhnologiya, oborudovanie, instrumenty) = Metal Working and Material Science*, 2022, vol. 24, no. 4, pp. 219–242. DOI: 10.17212/1994-6309-2022-24.4-219-242. (In Russian).

*** Corresponding author**
Kutkin Oleg M., Student, Laboratory assistant
Novosibirsk State Technical University,
20 Prospekt K. Marksa,
630073, Novosibirsk, Russian Federation
Tel.: 8 (962) 811-59-27, **e-mail:** kutkino@list.ru

Introduction

A "new age" in the field of materials research is believed to have begun with the discovery of X-rays in 1895 and X-ray diffraction in 1912. This type of rays turned out to be a powerful tool for revealing structural features of materials at different scale levels. For a period of slightly more than 100 years, dozens of research methods based on the use of X-rays have been proposed. Most analytical instruments use X-ray tubes as radiation sources. The number of such devices produced in various countries is huge and it is very difficult to estimate it.

Particle accelerators and specialized synchrotron radiation sources represent a special type of expensive and, by many parameters, unique analytical equipment. Synchrotron radiation (*SR*) is an electromagnetic oscillation created by ultrarelativistic electrons as it moves along a curvilinear path under the influence of a magnetic field. When moving along a circular orbit, the radiation has an intensity distribution in the form of a cone with a divergence angle $\gamma^{-1} = \frac{E}{mc^2}$, rad. The maximum power of the emitted radiation is accounted for by the frequency:

$$\nu_{\max} = \frac{3}{2}\left(\frac{E}{mc^2}\right)^3, \text{ Hz}$$

where $v_{\max}$ is the radiation frequency; E is the total electron energy; m is the electron mass, c is the speed of light.

By changing the electron path, it is possible to vary the maximum radiation in a wide range of the electromagnetic scale. Synchrotron radiation has a high degree of linear polarization in the plane of the electron orbit and a higher intensity compared to the radiation of X-ray tubes [1].

The first sources of *SR* were charged particle accelerators which produced a spurious synchrotron radiation. When revealing the advantages of synchrotron radiation and increasing the number of problems solved while using it, it turned out that it made sense to create specialized *SR* sources in which the analyzed radiation was not spurious, but main and useful.

The unique parameters of *SR* determine its enormous advantages over other sources, including X-ray tubes. Higher photon fluxes provide higher resolution at an equivalent exposure time by reducing the size of the X-ray detector pixels or by changing the size of the X-ray beam.

One of the methods based on the use of synchrotron or X-ray radiation is computed tomography (*CT*) which makes it possible to obtain images of the sections of the objects by processing multiple absorption X-ray patterns. When implementing the analyzed method, the computer ensures the operation of the X-ray source and processing of the data recorded by the detector. The advantages of using a synchrotron source with this method of image visualization include the parallelism of the rays, high radiation brightness values, that leads to reduction in data collection time and improvement in contrast when monochromatic radiation is used.

With tomography it is possible to obtain three-dimensional pictures of objects for its further analysis. Computed tomography shows very good results when examining compact (isometric) samples. At the same time some limitations appear while implementing this research method. Firstly, the maximum possible access to the object of research is necessary to ensure the quality of the obtained images. The second limitation is related to the fact that in order to prevent excessive absorption of radiation the dimensions of the object have to be small. If these conditions are not met, artifacts appear in the images in the form of distortions that do not correspond to the real object. In order to reduce the number of artifacts that occur during the implementation of the computed tomography method, the sample should be stretched by a value less than the effective field of view of the 2D detector in all directions perpendicular to the rotation axis. Taking into account this circumstance, the analysis of cylindrical samples is the most rational [2].

These problems can be solved by using either the method of laminography or tomography with a limited angle. Meanwhile, the limited angle tomography method has disadvantages which were considered in the work of *Helfen et al.* [3]. The review presented below is focused on the synchrotron laminography method for the analysis of metal alloys.

Methods for studying flat samples. Tomography and synchrotron laminography

One of the possible approaches to the problem of studying non-compact (non-isometric) samples is based on the idea of synchronous movement of the X-ray source together with the detector around a stationary object. This approach was proposed in 1932 by *Ziedses des Plantes* and the method based on it was called planigraphy [4]. In accordance with this method a set of X-ray patterns obtained in one scanning cycle is used to obtain an image of one section of an object located in the focal plane. This concept underlies the method of classical tomography (also called the laminography method); while implementing this method it is necessary to change the position of the object of research along the vertical in order to obtain images of different sections. Despite its simplicity, the method is fast and the images are of good quality (resolution).

In the 1970s this approach [5] began to be used in medicine to examine human patients. The adapted principle of classical tomography (laminography) was used in the first generation of medical tomographs (Fig. 1). Brain was studied by the first devices (Fig. 2). It should be noted that the pixel size was 3 mm (in modern devices – 30–200 μm). Compared to modern tomographs, the image shown in the figure is characterized by a rather low quality. Its analysis does not allow us to obtain complete information about the patient's condition.

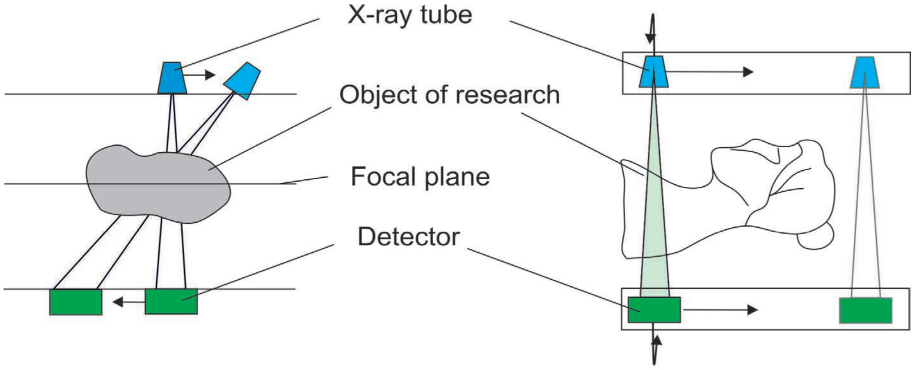

a *b*

Fig. 1. Scheme of classical tomography (*a*) [6] and scheme of the first generation tomograph (*b*) [7]

Various classifications of tomographs have been proposed in literature. According to one of these classifications there are five generations of tomographs (Fig. 1, *b* and Fig. 3) [7] which differ in design solutions and the number of projections recorded by the detectors.

When using first-generation scanners, images were obtained by moving one highly directed X-ray tube and one detector along the frame layer by layer. After 160 measurements the frame was rotated through an angle of 1° in the axial direction and the state of the next layer was analyzed. Measurement of the radiation intensity during the analysis of each layer lasted ~4.5 minutes and the imaging took ~2.5 hours.

The second generation scanner (mid-1970s) (Fig. 3, *a*) used a tube that formed a fan-shaped X-ray beam in combination with several detectors, which were opposite each other while rotating around the patient. Because of using a fan beam and several radiation detectors the angle of rotation in devices of this type increased to 30°. In this case, as well as in the devices of the first

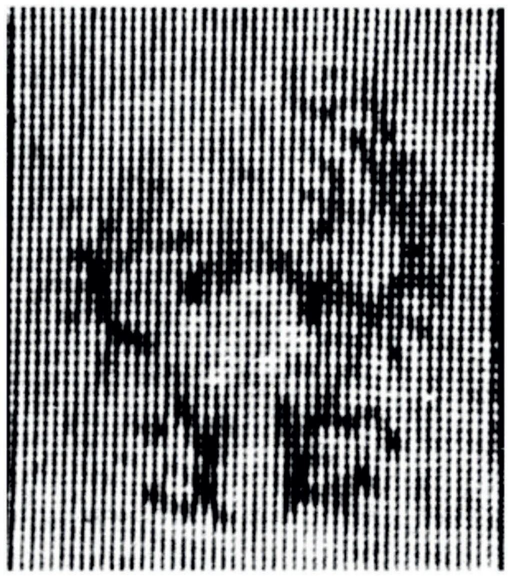

Fig. 2. The first image of the brain obtained by tomography [8]

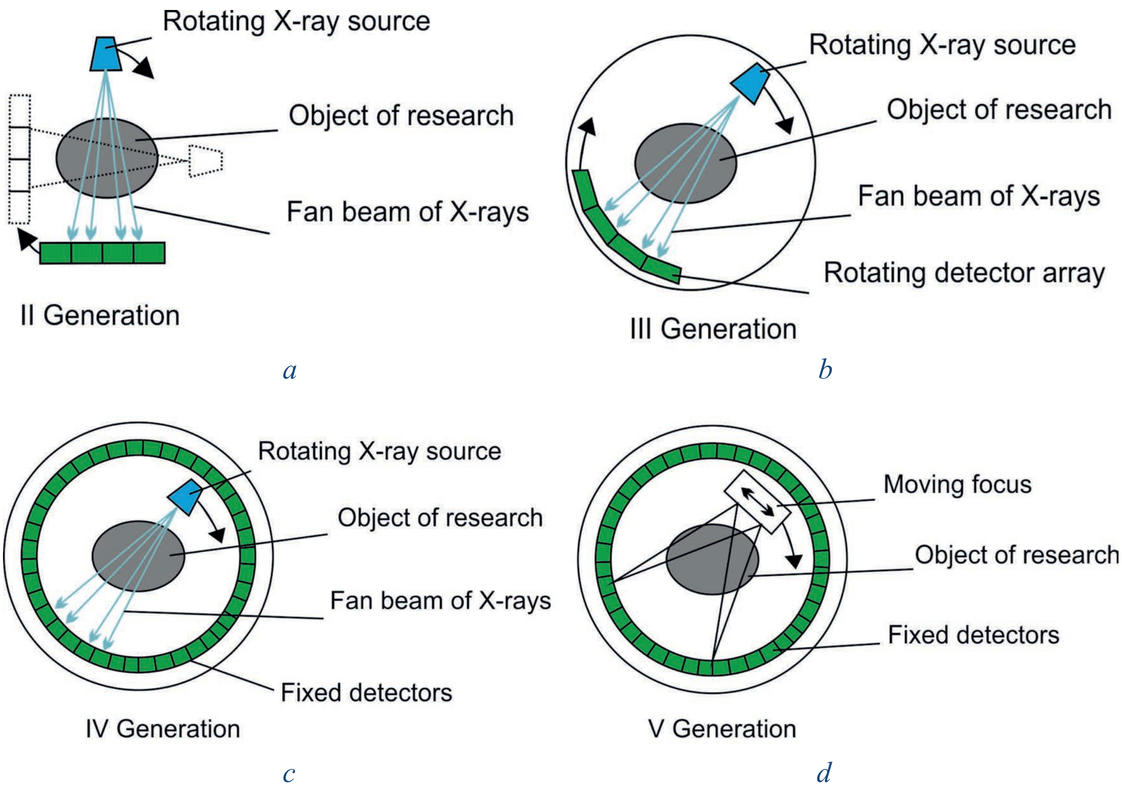

Fig. 3. Schematics of several generations of tomographs [7]

generation, the principle of parallel scanning was used. The measurement time required to obtain one image was ~18 seconds.

Devices of the third generation began to use the principle of spiral movement of the x-ray tube and detectors of radiation that passed through the patient. One step corresponded to the linear displacement of the table by a certain amount. In this case the tube and detectors simultaneously rotated one full turn around the patient lying on the table. This technical solution allowed reducing the research time significantly. The number of detectors also increased (up to ~700 pieces). Using third-generation devices made it possible to examine the patient's abdominal cavity and lungs.

In the design of tomographs corresponding to the fourth generation, a set of fixed detectors (1,088 luminescent sensors) was located in the form of a ring (around the patient). Scanning time (when obtaining 1 image) decreased to 0.7 seconds [7].

The main feature of the fifth generation devices (early 1980s) is the use of a fixed electron beam gun. In the process of shooting the electron beam is focused and directed to a tungsten target located under the patient's table. High-speed solid-state detectors are located in front of targets in the form of an arc with an angle of 216°. There are no significant differences in image quality compared to the previous generation of equipment. At the same time, the scanning time decreased to 33 ms. Such tomographs can be used to study the heart.

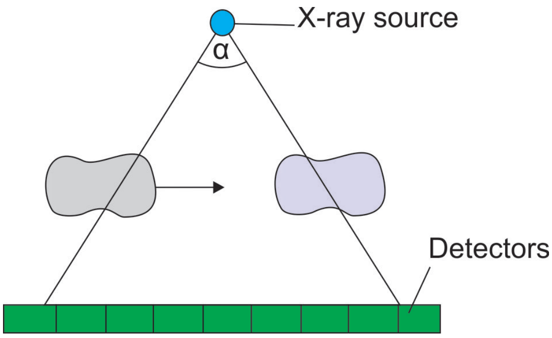

Fig. 4. Implementation of the laminography process according to the scheme proposed by *J. Zhou* [6]

Zhou et al. [6] presented a new approach to apply laminography to materials. In accordance with this approach the analyzed object moves linearly relative to the fan beam created by the microfocus X-ray tube (Fig. 4). This solution makes it possible to obtain data corresponding to rotation through the angle α for an object located in a parallel beam.

The method proposed by *Zhou et al.* has a number of advantages over classical tomography. In one scan it allows to get an image of the entire volume of the sample. Its practical implementation provides improved image quality of sections (without blur effect).

The principles of radiation formation when using synchrotron sources and X-ray tubes differ significantly. For this reason other technical solutions have been proposed for *SR* sources that make it possible to obtain tomographic images. The Synchrotron radiation computed tomography (*SRCT*) method assumes that the sample rotates around the axis perpendicular to the X-ray flux (Fig. 5, *a*).

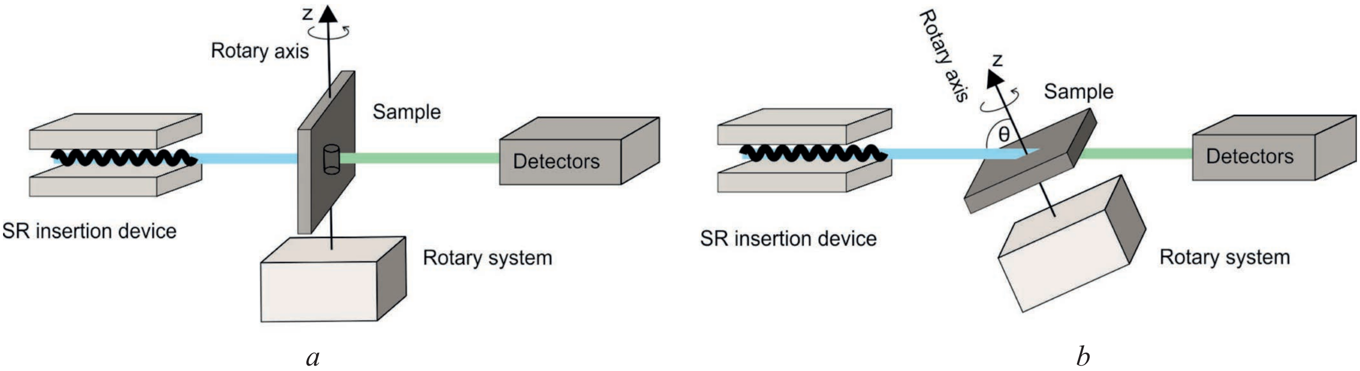

Fig. 5. Schematics of setups, implementing the principle of tomography (*a*) and laminography (*b*) [12]

Problems that arise when obtaining data from non-compact (non-isometric) samples can be avoided by using the method of Synchrotron radiation computed laminography (*SRCL*) which was proposed in 2005 by *Helfen et al.* [9]. Using a facility compatible with a stationary synchrotron source (*ESRF*, *station ID19*), they developed a method for collecting data on the structure of the analyzed object.

The *SRCL* method combines the principles of laminography with the advantages of synchrotron imaging. Currently, it is used for non-destructive testing of non-isometric objects on a number of synchrotron radiation sources (*ESRF*, *ANKA*, *Spring-8*).

When implementing the *SRCL* method, the rotary axis is deflected by an angle θ with respect to the direction of the X-ray beam (Fig. 5, *b*). This decision which affects the image quality makes it possible to reduce the distance from the sample to the detector. The tilt angle θ is determined experimentally. In this case the maximum rotation of the axis is usually limited by the design capabilities of the goniometer that holds and rotates the sample. The research results obtained using the *SRCL* method are comparable with the data that can be recorded by digital tomosynthesis [10, 11].

Helfen et al. thought that the *SRCL* method could be perceived as a more generalized version of the *SRCT* method [2]. Based on this fact and the similarity in the design of the equipment, the methods of computed laminography and tomography can be implemented on the same unit. *Fisher et al.* [13] demonstrated this possibility using a laboratory X-ray source. It was shown that tomographic research methods, including those based on the use of phase contrast [14], could also be applied to laminography.

The method of computed laminography implies the need to use equipment which includes an X-ray source, a turntable with an inclined axis, a system of detectors and a computer with a software package for data processing. Depending on the task, technical solutions can be implemented that provide any additional effect (tensile, torsion, heating of the sample, impregnation of the fibrous composite, etc.). In the following sections of the paper, examples of the use of such setups are given.

Resolution of synchrotron radiation computed laminography

As mentioned earlier, when using tomography full access to the object under study is required, the size of this object is smaller than the size of the detector. Otherwise, the quality of the resulting image will deteriorate. This circumstance limits the application of the *SRCT* method to the study of large, non-isometric samples, such as plates. The reason for blurring (deterioration of quality) of the image and the appearance of artifacts is a lack of data that is required for accurate restoration of the section. Restoration of images in the absence of a certain fraction of data can be performed using the reciprocal space (three-dimensional *Fourier* space) (Fig. 6) [2]. However, it should be taken into account that synchrotron computed

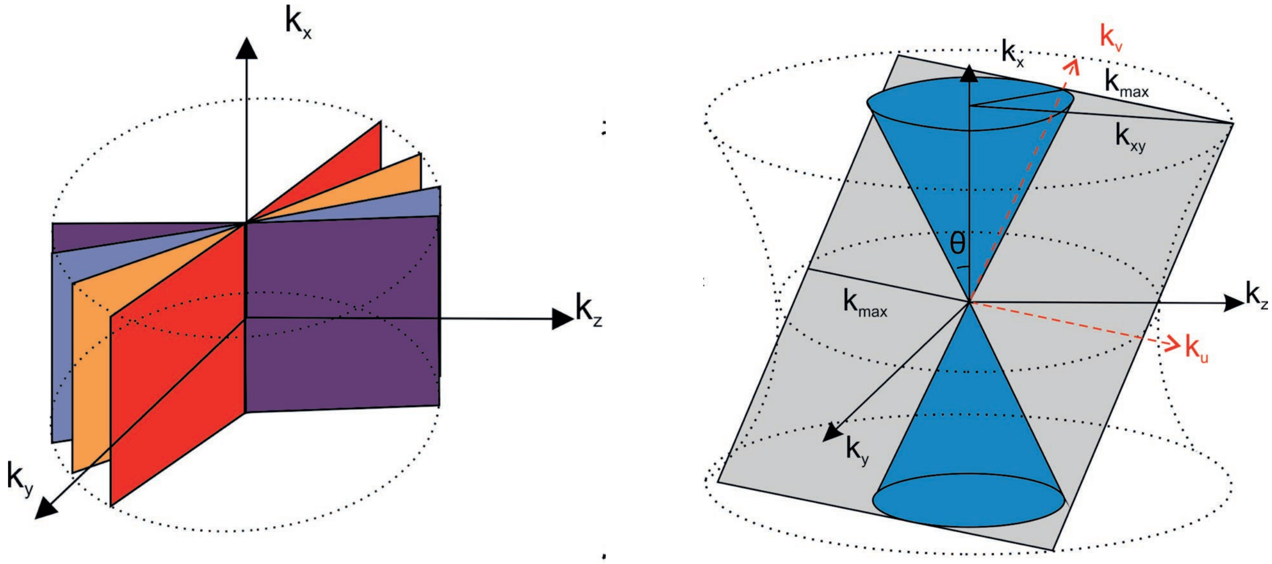

a *b*

Fig. 6. Reciprocal space regions obtained using the Fourier transform:
a – SRCT-scan; *b* – SRCL-scan. Cones of missing information are marked in blue [2]

laminography provides the best spatial resolution in those directions along which there is no data loss, i.e. outside the missing cones.

The sample axis direction k_z highlighted in Fig. 6 is oriented parallel to the incident X-ray beam. The reciprocal space region obtained after the *Fourier* transform of one two-dimensional projection and highlighted in Fig. 6 b in gray is a plane parallel to the vectors $\boldsymbol{k}_u$ and $\boldsymbol{k}_v$. When constructing a large number of projections, the analyzed area forms a rotationally symmetric body, the outer contour of which has the form of a hyperbolic surface described by the equation:

$$k_{xy}^2(k_z) = k_{\max}^2 + k_z^2 \tan 2\Theta ,$$

where $k_{\max} = \dfrac{1}{2s_p}$, s_p – pixel size.

Fig. 6, *b* shows that there are no two cones with an opening angle of 2θ. This is explained by the tilt of the rotation axis when implementing the *SRCL* method. The loss of information in one direction due to the lack of a certain amount of data can be compensated by an increase in spatial resolution in other directions. The use of monochromatic radiation in the implementation of the *SRCL* method is a factor that ensures high spatial resolution up to micron and submicron scales. The maximum resolution of the method is determined by the characteristics of the detector. Using nanolaminography, images with a resolution of ~100 nm were obtained [15].

If spatial resolution is not a defining requirement, neutron laminography can be used which has the advantage of being sensitive to chemical elements other than X-rays. Features of the adaptation of the laminography method for neutron imaging are presented in [12].

Comparison of laminography and tomography methods. Augmented laminography method

When using the method of computed laminography, an isotropic beam scanning scheme is implemented which provides the same resolution and sensitivity in directions perpendicular to the axis of rotation. As mentioned earlier, this characteristic of the *CL* method gives excellent results compared to the limited angle *CT* method.

The advantages of the *CL* scheme are as follows:

– full 360° rotation is available even for large sample;

– constant tilt of the sample during analysis provides a close average value of the intensity of the transmitted radiation;

– the rotational symmetry of the accessible *Fourier* region is a factor contributing to the further reconstruction of the image.

These advantages have been demonstrated by *Feng Xu et al.* [3]. In those cases when implementing the *CT* method a limiting angle occurs after which it is not possible to obtain an image of the sample the *CL* method can be used. It is noted that artifacts in the image of the sample surface in the direction of the normal to the movement of X-rays in the implementation of the *CT* method limit the achievable resolution to a greater extent than in the *CL* method. In addition, when implementing computed tomography, non-isotropic artifacts in these planes create more noticeable distortions in the images compared to isotropic artifacts from *CT*.

One of the advantages of the method of synchrotron computed tomography over synchrotron computed laminography is the ability to select the optimal signal/noise ratio – the number of artifacts after scanning the object. If it is possible to scan the sample with a rotation of 360° using the *CT* method so in this case it is possible to select such an amount of experimental data that will allow one to reconstruct the image with a higher signal-to-noise ratio and fewer artifacts. The advantages of the *CL* method make it suitable in cases where the range of the missing angle limited by the geometry of the sample or the design features of the equipment is large for the *CT* method.

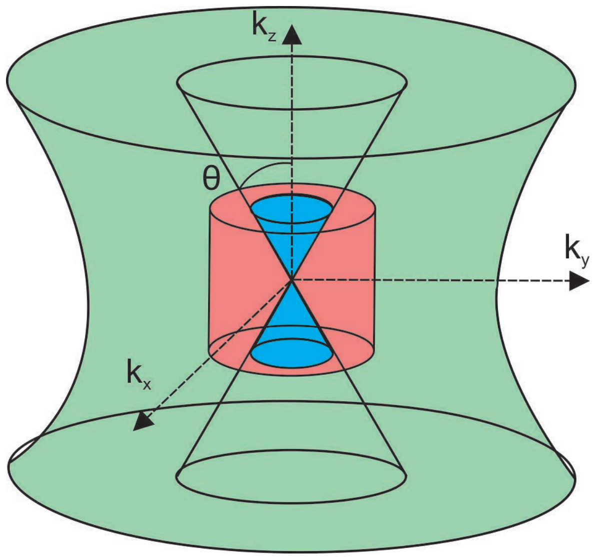

Fig. 7. Sampled areas in the Fourier space of the reconstructed volume. The green volume outside the two inner 2θ cones refers to CT laminography and the red volume refers to low-resolution CT. The blue volume corresponds to the area, where missing information in the laminography data can be reconstructed using CT [16]

Zuber et al. developed the augmented laminography method [16], which uses X-ray tubes as radiation sources. Its merits were demonstrated in the study of fossils. This method is a combination of both types of scanning: *CT* and *CL*. Its idea is to supplement the *Fourier* space of laminography with information obtained using computed tomography with a lower resolution (Fig. 7). However, when examining elongated samples, some regions of the *Fourier* space are still missing due to the larger field of view and, as a result, the low resolution typical for computed tomography of such objects. The implementation of the augmented laminography method implies the need to increase the field of view when scanning a sample with zero tilt. This is due to the condition of the *CT* scan.

To demonstrate the quality of images obtained using various research methods, Fig. 8 shows the results of the analysis of test samples which consisted of several layers, different in shape and materials [16]. The image of the *x–y* plane obtained by the *CL* method is characterized by good resolution and quality. The resolution of the analyzed plane, reconstructed by the *CT* method, is noticeably worse. The augmented laminography method demonstrates the most qualitative result.

When considering the *x–z* plane using the computed laminography method, artifacts that distort the structural features of the analyzed object significantly are noted. The image obtained by computed tomography doesn't have this drawback. At the same time, as well as the image in the *x–y* plane, it is characterized by low spatial resolution. The reconstruction obtained using the augmented laminography method (Fig. 8) is characterized by the absence of significant artifacts and high resolution. Table 1 presents the main characteristics of these three methods.

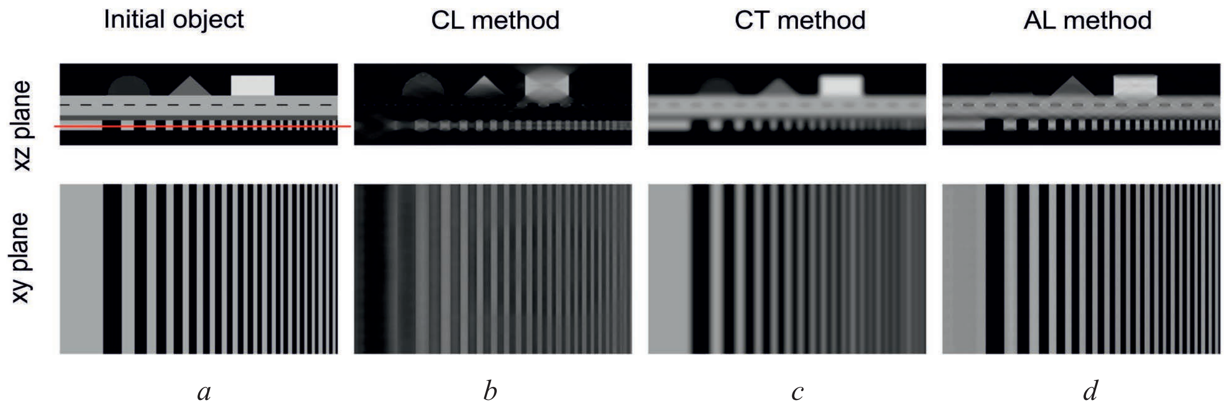

Fig. 8. Comparison of different object scanning methods. The laminography is implemented at an inclination angle of the sample θ = 29.8°. In diagram *a* the *x*–*y* plane is marked with a red line [16]

Table 1

Comparison of tomography, laminography, and augmented laminography methods [16]

Computed tomography	Augmented laminography	Computed laminography
+ High resolution in the *x*–*y* plane	+ High resolution in the *x*–*y* plane	+ Equal resolution along the *x*, *y*, *z* axes
+ A significant geometric increase can be achieved	+ Typical *CL* artefacts are largely suppressed (intermediate between *CL* and *CT* *z*-direction resolution)	− Sample must fit the field of view
− Blurring in the *z* direction	− Increased scan time	− Strong attenuation for large objects

Implementation of the laminography method

The tilt angle of the rotary axis θ in the implementation of the *SRCL* method is related to the geometry of the samples and determined experimentally in each case. In order to achieve the required resolution the value of θ has to provide the optimal average value of the intensity of the transmitted radiation.

The energy of X-ray radiation is calculated based on the characteristics of the material, namely, taking into account the radiation absorption index. Monochromatic X-ray radiation passing through any medium when interacting with atoms or molecules attenuates according to the *Bouguer-Lambert-Beer* law:

$$I = I_0 e^{-k_\lambda l}, \tag{1}$$

where I_0 is the intensity before passing through the medium with thickness l; I is the intensity at the exit from the medium.

The dependence of the absorption index k_λ on the wavelength of the absorbed radiation is called the absorption spectrum of the substance.

In cases where the sample consists of several materials based on the absorption capacity it is necessary to select the energy level that provides optimal image contrast. In this case the absorption index is determined by the expression:

$$k_\lambda l = \int_L f(x, l)\, dl, \tag{2}$$

where $f(x, l)$ is the linear absorption coefficient of the material, dl is the element of the absorption path along the beam L.

Based on dependences (1) and (2), having determined the absorption function on the basis of experimental data, it is possible to restore the image of the volume of the body under study. To do this, you need to solve an equation of the form:

$$\ln \frac{I_0}{I} = \int_L f(x, l)\, dl. \tag{3}$$

Currently, to solve this equation, software packages that allow to reconstruct images of the objects under study based on tomography or laminography data with filtered back projection methods [17] (based on the *Radon transform*, *Algebraic Reconstruction Technique*, etc.,) are used.

Examples of laminography application for the analysis of metal alloy samples

Computed laminography was used originally as a method for studying elements of microsystem technology, namely printed circuit boards. Its application to solve this problem is relevant at the present time. Later, the method was used in the study of cultural heritage objects [18, 19], in paleontology [20], materials science [21], and other research areas.

In materials science the laminography method is in demand for solving problems related to the study of objects made of polymer composites [22] and metal alloys. The effect due to the phase contrast can be used to highlight interfaces between different materials with poor absorbency. The essence of the proposed solution is to change the distance from the radiation source to the sample which ensures the appearance of interference effects on the detector. This approach helps to improve the sharpness of the boundaries of the sample components.

Examples of using the laminography method for the analysis of a number of alloys are discussed below.

In situ studies of plastic deformation of metal plates

The method of computed laminography provides a unique opportunity to represent the mechanisms of crack propagation in sheet materials and fixation of internal damage in three dimensions of the sample. In some works synchrotron computed laminography was used to study the processes of crack formation and destruction of metal plates [23–27]. Fig. 9 shows a diagram of one of the devices used for loading samples with stress concentrators.

Figure 10 shows the diagram of *station ID19* located at the *European Synchrotron Radiation Facility* (France) equipped with devices for implementing the laminography method [28]. This station was used to study the mechanisms of destruction and development of cracks in aluminum alloy samples with a loading device (Table 2) [29]. Figure 11 shows the scheme of deformable samples. During the tests the volume of formed defects, its reorientation and sizes according to *Feret's* shape factor were evaluated.

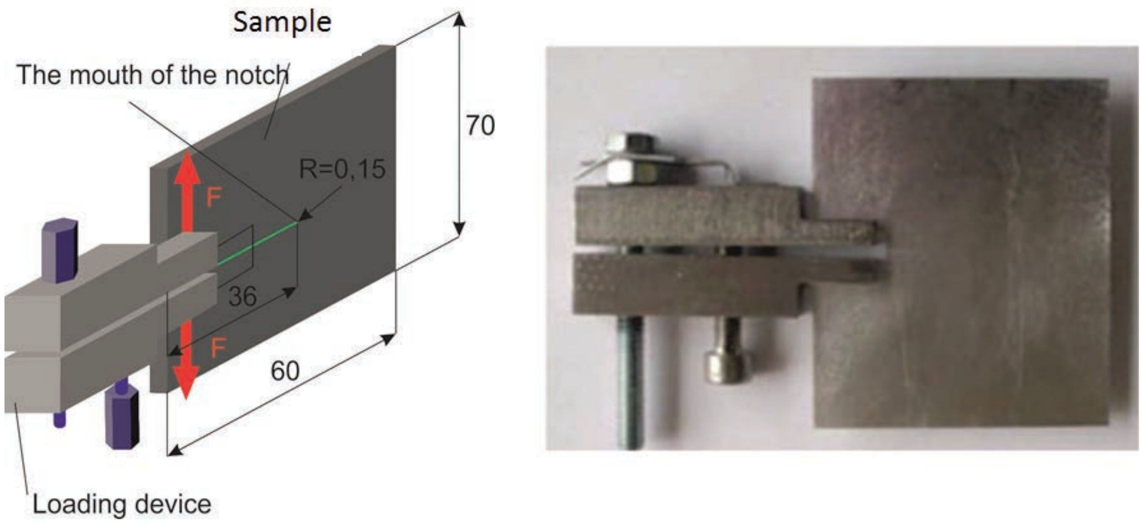

Fig. 9. Schematic of the device used for loading a specimen with a stress concentrator [27]

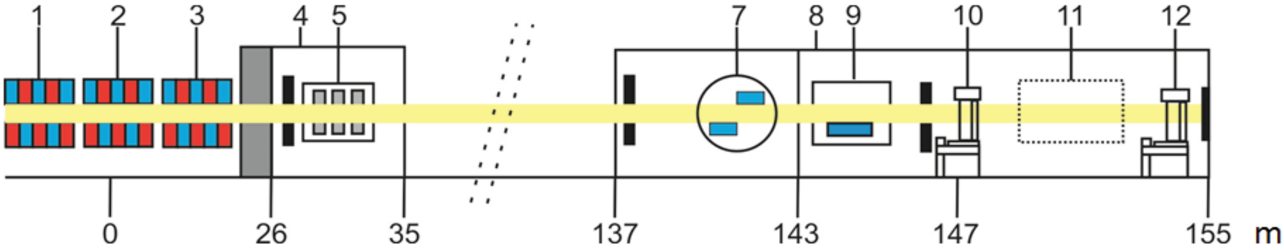

Fig. 10. Main elements of *ID19*:

1 – undulator *U32*; *2* – wiggler *W150*; *3* – revolver *U32/U17*; *4* – Optics Hutch 1; *5* – attenuators; *6* – Optics Hutch 2; *7* – double-crystal monochromator; *8* – Experimental Hutch; *9* – multilayer monochromator; *10* – high-resolution tomograph; *11* – Custom: space for additional instruments, such as a laminograph, horizontal diffractometer, etc: *12* – medium-resolution tomography [28]. The lower row of numerical values corresponds to the distance from the radiation source, in meters

Table 2

Composition of aluminum alloy (wt. %)

Si	*Fe*	*Cu*	*Mn*	*Mg*	*Cr*	*Zn*	*Ti*	*Al*	Rest
≤0.5	≤0.5	3.8–4.9	0.3–0.9	1.2–1.8	0.1	0.25	0.15	90.7–94.7	0.05–0.15

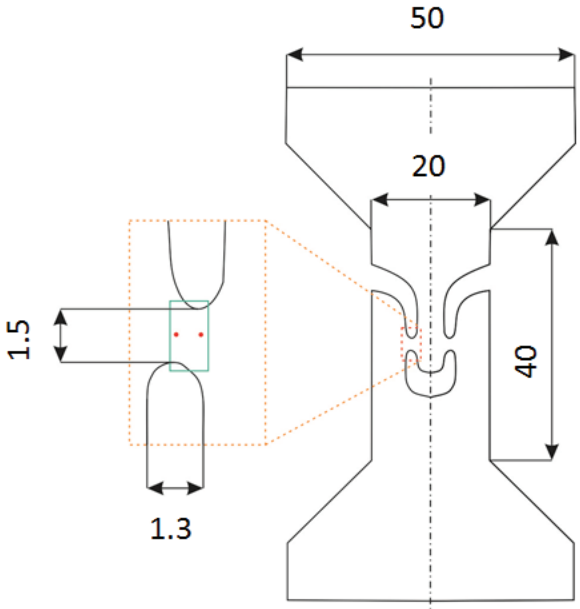

Fig. 11. Sketch of the specimen with the selected area. The red dots denote the position of the extensometer used to measure the displacement of the deformable zones [30]

When studying materials with laminography, the axis of rotation of the sample was tilted with respect to the direction of the X-ray beam at an angle of ~65° (Fig. 12). A pink beam from an undulator (period 13 mm) with a peak X-ray energy of ~26 keV, which was filtered with an aluminum plate 5.6 mm thick, was used for this research. These parameters provided a compromise between the penetrating power of X-rays and the contrast of the generated image [31]. During the research the sample mounted in the grips of the tensile machine rotated 360°. A single rotation step was 0.1°. Thus, the process of scanning one sample involved obtaining and subsequent processing of 3,599 X-ray patterns. The exposure time for each X-ray was 50 ms. X-ray patterns were processed using the filtered back projection algorithm to reconstruct the 3D image [32]. In addition to the statistical processing of defects in the structure of the material, an in-depth

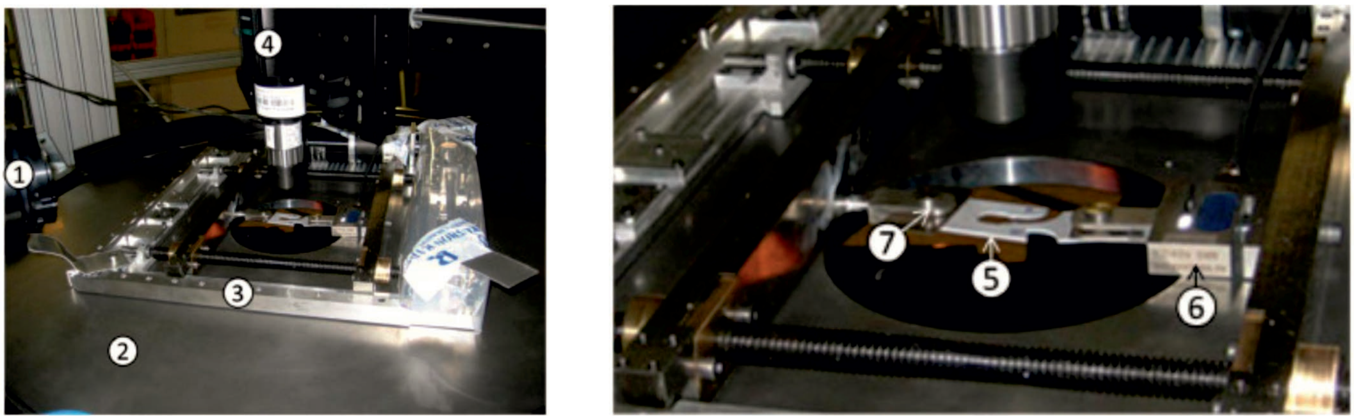

Fig. 12. Experimental setup for laminography of flat samples during stretching:
1 – X-ray detector; *2* – Rotating laminography platform; *3* – Electro-mechanical in-situ tensile machine; *4* – Optical microscope; *5* – Shear specimen (broken); *6* –Load cell (5 kN); *7* – Loading pin [29]

analysis of the damage mechanisms leading to the final destruction of the loaded samples was carried out in the work. It was established that the process of material destruction was associated with the behavior of the intermetallic particles which were contained in it. Using the laminography method, the authors of the work identified two stages in the development of the destruction process. At the initial stage, a crack was formed inside the particle during the deformation process. This crack was perpendicular to the direction of maximum principal stress. Further, these cracks opened in the process of loading the sample that led to the appearance of large cavities. Combining the results of studies obtained by the methods of laminography and fractography of samples, conclusions were drawn about the mechanism of destruction of the alloy under external loading. The results of additional modeling by the *REV* (representative elementary volume) method showed that the opening of pre-cracked particles led to strain concentration at the mesoscopic level which ultimately led to the formation of strain bands.

Visualization of pores developing during plastic deformation

The work of *Isshin Ando et al.* [33] performed at the *BL20XU station* at the *Spring-8 source* (Japan) [34] can be mentioned as an example of visualization of pores that arise during the plastic flow of a material. The objects of study were samples obtained by sintering pure iron powder (*JFE Steel Co., JIP301A*). The porosity of the study objects (including open and closed pores) was 11.7 %. Samples with dimensions of $3\times2\times1$ mm^3 were deformed according to the tensile scheme.

The equipment of the *BL20XU* station made it possible to conduct studies with a maximum spatial resolution of 1 μm for subsequent volume reconstruction with a minimum voxel size of 0.3 μm. The photon energy of a monochromatic X-ray beam generated by a double-crystal *Si* (111) monochromator cooled by liquid nitrogen was 37.7 keV. The axis of rotation of the sample was tilted at an angle of 45° to the X-ray beam. The detector was located at a distance of 18.0 mm from the center of rotation located on the surface of the sample. X-ray patterns with a diameter of 1,000 μm were obtained with an exposure of 300 ms at a rotation of 0.1° (for each image). The images were reconstructed by processing multiple X-ray patterns using a filtered back projection algorithm and rendered as 3D images using *Avizo 9.1.1* software (FEI Co.).

The *SRCL* method was used to analyze the initial (undeformed material) as well as samples deformed according to the tension scheme at a rate of 10^{-3} s^{-1}. We studied five plastically deformed samples in different structural states (after deformation with different degrees). In the research a quantitative assessment of the pore configuration was carried out. The transformations of pores occurring at increased values of deformation were tracked using the methods of algebraic topology and persistent homology [35]. An approach based on the use of the laminography method made it possible to describe the process of coalescence of pores in iron samples obtained by powder metallurgy.

Post-mortem testing of alloys

The laminography method can also be used to study materials that have previously been subjected to various types of external actions. In these cases there is no need to install any additional equipment on the station.

Deformation and failure of magnesium alloy

Kondori et al. [36] presented the results of a study of the *AZ31B* magnesium alloy by the laminography method. Samples cut from a 32 mm thick hot-rolled plate (Fig. 13 *a*, *b*) were subjected to uniaxial tension in a servo-hydraulic machine. One sample was deformed to failure; the other was deformed to the stage corresponding to a significant drop in load.

The sections of the rods obtained in the *EDM* machine (Fig. 14, *c*) were examined by laminography at the *ID19 ESRF station*. The mechanisms of accumulation of post-embryonic damage and its role in the formation and growth of macroscopic cracks were studied.

The tilt angle of the rotation axis of the objects was ~25°. The studies were carried out using monochromatic radiation with a photon energy of 25 keV. The minimum distance from the sample to the detector was

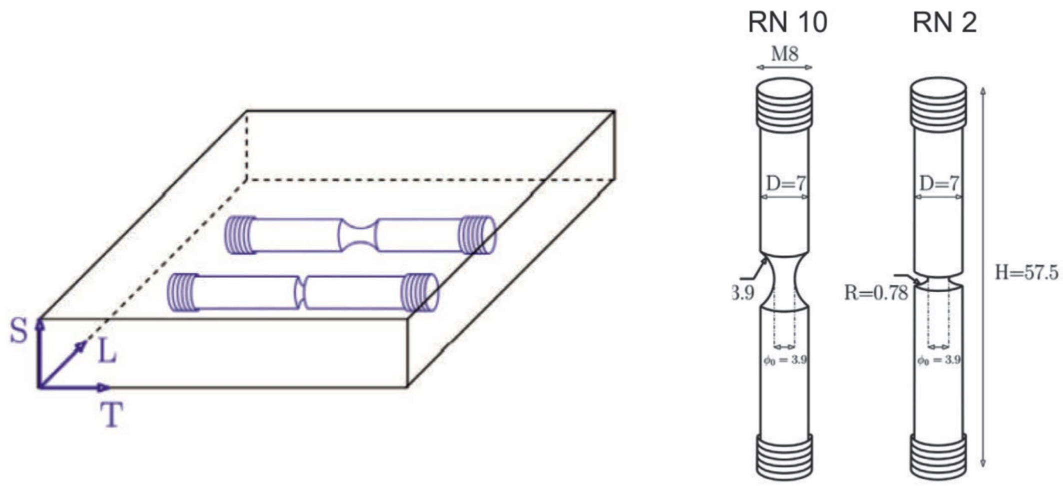

a *b*

Fig. 13. Samples (*RN*10 and *RN*2) (*a*) orientation in the plate and its geometry (*b*) [36]

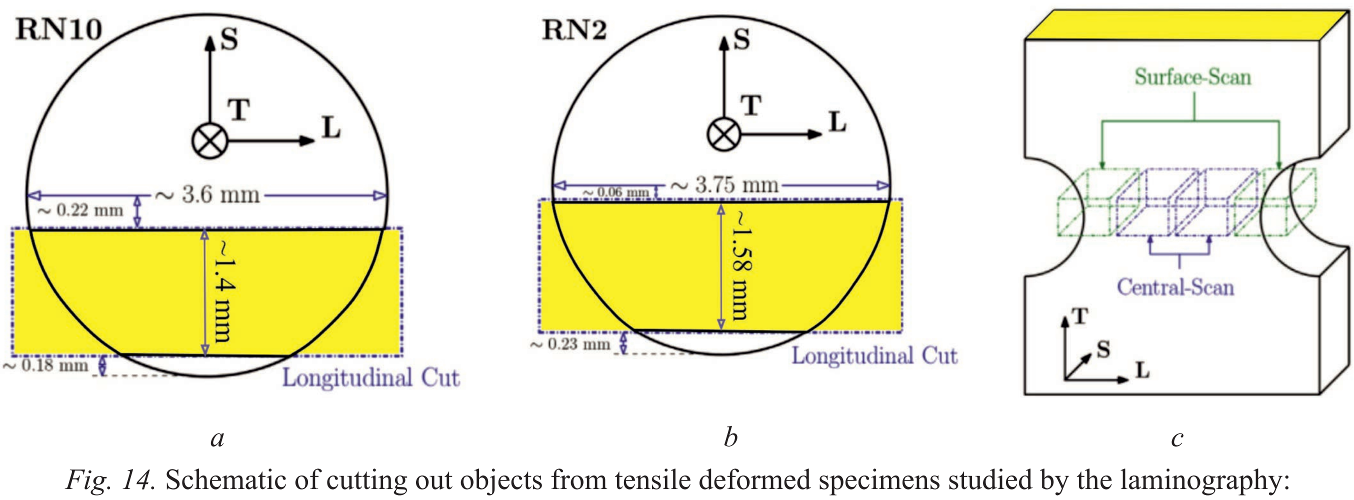

a *b* *c*

Fig. 14. Schematic of cutting out objects from tensile deformed specimens studied by the laminography:
a, *b* – top views showing the dimensions and relative location of two longitudinally cut plates; *c* – view of a single plate with four study areas labeled as Surface-Scan and Central-Scan [36]

70 mm, which led to an improvement in the quality of object boundaries due to the appearance of phase contrast. The scanned area had a size of 1 mm^3 with a voxel size of 0.7 μm. The exposure time for each projection was 250 ms. The analysis of 1,500 X-ray patterns allows to reconstruct these sizes.

An analysis of ~1,000 voids corresponding to each image recorded by laminography was made with the *ImageJ* software to quantify the size and shape of defects accompanying the initiation of cracks. All measurements were carried out on images parallel to the *T–L* plane at different sample thicknesses. The analyzed area was 31 mm^2 for the *RN10* samples and 36 mm^2 for the *RN2* samples (the geometry of the samples was described in [38]). The area occupied by each void was calculated taking into account its elliptical shape. The total defect fraction was defined as the ratio of the area of voids to the total area analyzed (excluding macrocracks). Geometric parameters of macrocracks were determined individually.

An analysis of the results obtained with laminography made it possible to reveal a number of features of the destruction of the *AZ31B* alloy, which can appear when loading other magnesium-based alloys [36]. Analysis of the behavior of the material in the process of stretching indicates its plasticity. The voids that have arisen during loading are distributed over the entire deformable region of the sample. Damage occurs in the form of flat voids, the size of which is determined by the spatial position, the level of local deformation, and the nature of the stress strain state of the material. The transition from the stage corresponding to the formation of small-sized voids distributed in the volume to the final destruction of the sample occurs through the appearance of macroscopic cracks when the voids merge in the direction of rolling the plate. When several parallel macrofractures occur away from the mouth of the notch and merge together a stepped (corrugated) surface is formed. Based on the studies a conclusion was made about the necessity of further research of the crystallographic aspects of damage development in magnesium alloy samples at a higher spatial resolution.

Visualization of fatigue cracks

The method of synchrotron computer laminography can also be used to study fatigue cracks that appear in deformable materials. As an example, the results of studying such defects are given here. These defects occurred in a weld joint obtained by friction stir welding. The workpieces were made from aluminum alloy. Table 3 shows the composition of this alloy [38]. The tests were carried out at station BL19B2 of the SPring-8 source.

The materials studied in the work were subjected to low-cycle fatigue loading (3.37×10^5 and 4.8×10^4 cycles). The function of stress concentrators contributing to the fatigue cracks occurrence was performed by holes with a diameter of 0.3 mm. Figure 15 shows the dimensions of the analyzed samples.

During materials testing by laminography the axes of rotation of the samples were tilted by 30° with respect to the X-ray beam. At the output of the monochromator the X-ray energy was 28 keV. An X-ray detector (cooled *CCD* camera) recorded projection data every 0.5° (with a total rotation of 360°) with an exposure time of 400 ms per image. The sample was removed every 20 exposures and the response caused by the presence of the polymer was recorded to compensate for the attenuation of X-ray radiation caused by the acrylic tube to which the analyzed object was fixed.

The projection size fixed by the detector was 1,984×7,680 pixels (after 2×2 binning). Under these conditions there was a compromise between image resolution and simplicity of data processing. The effective size of the detector pixel was 5.7 μm (after binning). The size of the field of view was 11.3 mm (horizontal) × 4.4 mm (vertical). The X-ray beam was parallel at the length between the rotating magnet and the sample (52 m). The distance between the sample and the detector (0.8 m) ensured the manifestation of the phase contrast effect. The fracture images (Fig. 16) were reconstructed using the filtered back projection

Table 3

Composition of aluminum alloy (wt. %)

Si	*Fe*	*Cu*	*Mn*	*Mg*	*Cr*	*Zn*	*Ti*	*Al*
0.65	0.2	0.30	0.06	1.04	0.13	0.04	0.02	Rest

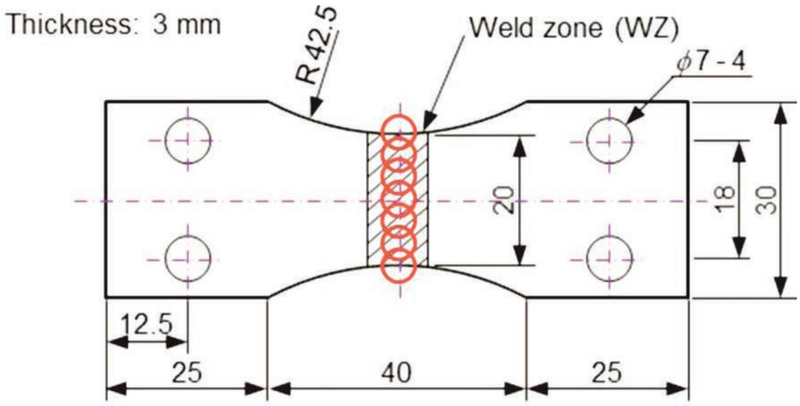

Fig. 15. Sample cut from a welded joint obtained by friction stir welding. The red circles are the fields of view of laminography [38]

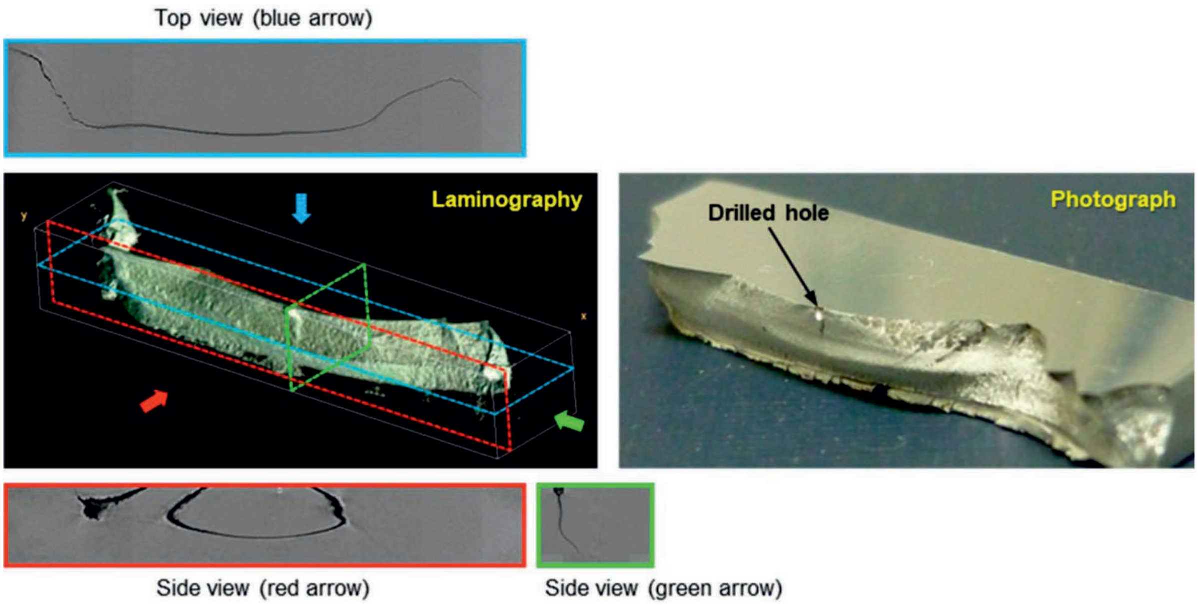

Fig. 16. The reconstructed synchrotron radiation computed laminography 3D image and a photograph of the fatigue crack [38]

algorithm and 3D visualization (Fig. 17) of seven hundred and twenty two-dimensional projections rotated relative to each other at an angle of 0.5°.

Images of cracks that appeared during external loading were successfully reconstructed. There is a good agreement between the calculated data and the actual data. The results obtained in the work allowed the authors based on the example of welded joints to conclude that the computed laminography method is highly effective for studying the processes of fatigue failure of materials. The information obtained by this method is important from the view of the development of materials characterized by a high level of fatigue properties.

Investigation of contact fatigue cracks

One of the applications of the method of synchrotron computed laminography is associated with the study of defects occurred in the process of contact fatigue loading [39–41]. Other methods of synchrotron studies including diffraction methods are also used to solve this problem [42, 43]. *Nakai et al.* [41] studied bearing steel. Table 4 shows the composition of this steel. Loading was carried out according to the rolling contact fatigue (Fig. 18). A 24×10×1 mm sample was cut from a forged and spheroidized ingot with a diameter of 65 mm. The increased sulfur content in steel made it possible to study cracks that appeared near

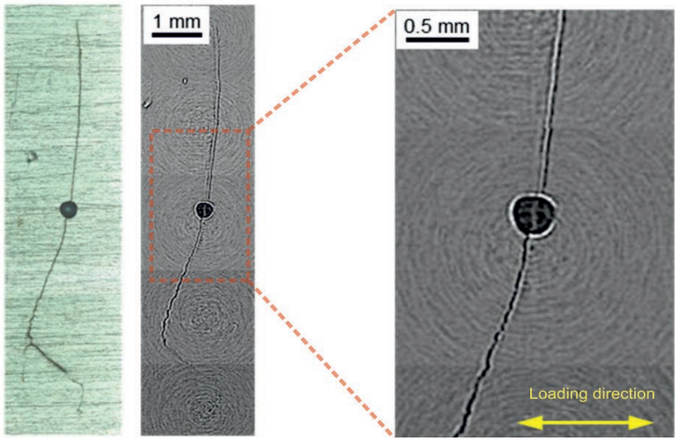

Fig. 17. The fatigue crack on the sample surface:
a – image obtained by light microscopy; *b*, *c* – images obtained by synchrotron radiation computed laminography [38]

Table 4

Composition of bearing steel (wt. %)

C	*Si*	*Mn*	*P*	*S*	*Cr*	*Fe*
1	0.35	0.47	0.006	0.02/0.049	1.5	Rest

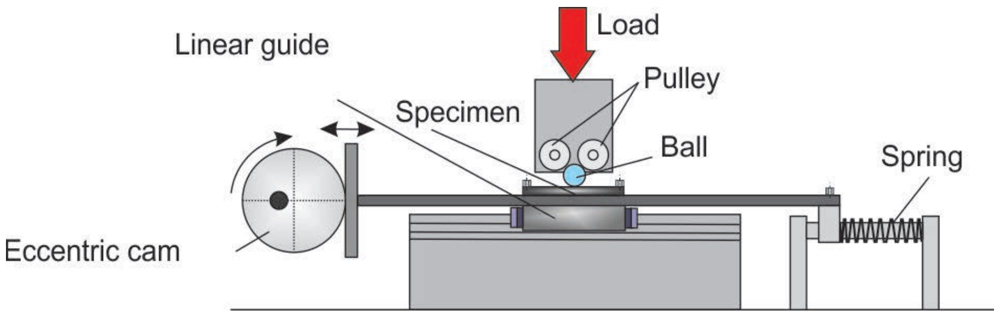

Fig. 18. Schematic of a contact-fatigue test setup [40]

MnS inclusions. Manganese sulfide inclusions are oriented perpendicular or parallel to the sample surface. Before testing, the samples were annealed with heating at 1,103 K for 0.5 h and then tempered at 453 K for 2 h.

Ceramic balls 6.0 mm in diameter with a *Young's modulus* of 300 GPa were used as indenters. The indenter performed multiple reciprocating movements over the sample surface. The length of the resulting friction track was 3.0 mm (Fig. 19) [39]. This paper presented the results recorded at the maximum *Hertzian stress* p_{max} = 5.39 GPa.

The works allowed drawing the conclusions about the duration of the initiation and propagation processes of vertical and horizontal cracks, as well as about the effect of the size and orientation of *MnS* inclusions on the processes of pitting in ball-bearing steel. The images of defects recorded by the laminography method made it possible to assess the nature of the material destruction at various stages of testing the samples. The analysis carried out by the authors of papers [39–41] indicates the effectiveness of the application of the computed laminography method using synchrotron radiation when studying the processes of contact fatigue loading of metals.

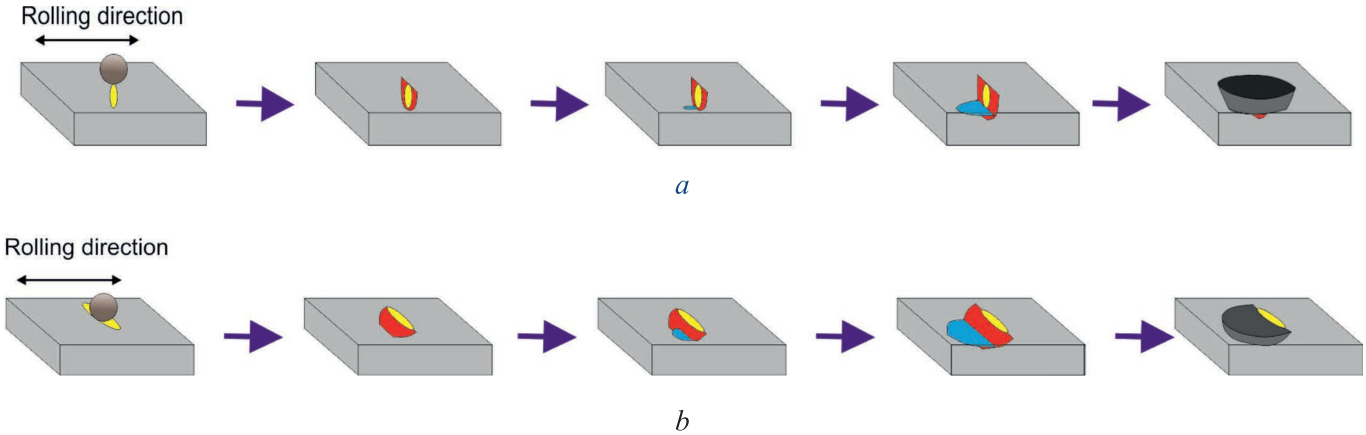

Fig. 19. Models of flaking mechanism from extended inclusion [39]:
a – sample with short vertical inclusions (low concentration of S); *b* – sample with horizontal inclusions

Conclusion

An analysis of the experiments based on using synchrotron radiation sources indicates the effectiveness of the methods of synchrotron computed tomography (*SRCT*) and synchrotron computed laminography (*SRCL*) when conducting research in the field of modern materials science. The *SRCL* method provides the possibility of monitoring the structure of materials when implementing various loading schemes including the study of fatigue and contact fatigue fracture processes. Implementation of the *SRCT* and *SRCL* methods is reasonable at the *Siberian Ring Photon Source,* which is under construction in Novosibirsk. The planned parameters of this source will make it possible to obtain images of the structure of structural and functional materials with high spatial resolution.

References

1. Ternov I.M., Mikhailin V.V. *Sinkhrotronnoe izluchenie: teoriya i eksperiment* [Synchrotron radiation. Theory and Experiment]. Moscow, Energoatomizdat Publ., 1986. 296 p.

2. Helfen L., Myagotin A., Mikulík P., Pernot P., Voropaev A., Elyyan M., Di Michiel M., Baruchel J., Baumbach T. On the implementation of computed laminography using synchrotron radiation. *Review of Scientific Instruments*, 2011, vol. 82, p. 063702. DOI: 10.1063/1.3596566.

3. Xu F., Helfen L., Baumbach T., Suhonen H. Comparison of image quality in computed laminography and tomography. *Optics Express*, 2012, vol. 20, pp. 794–806. DOI: 10.1364/OE.20.000794**.**

4. Ziedses des Plantes B.G. Eine neue methode zur differenzierung in der rontgenographie (planigraphies). *Acta Radiologica*, 1932, vol. 13, pp. 182–192. DOI: 10.3109/00016923209135135.

5. Hounsfield G.M. *A method and apparatus for the examination of a body by radiation such as X or gamma radiation*. Patent Specifications, 1283915. London, Patent office, 1972.

6. Zhou J., Maisl M., Reiter H., Arnold W. Computed laminography for materials testing. *Applied Physics Letters*, 1996, vol. 68, p. 3500. DOI: 10.1063/1.115771.

7. Marusina M.Ya., Kaznacheeva A.O. *Sovremennye vidy tomografii* [Modern tomography types]. St. Petersburg, ITMO University, 2006. 132 p.

8. Hounsfield G.M. Computed medical imaging. Nobel lecture, December 8, 1979. *Journal of Computer Assisted Tomography*, 1980, vol. 4, pp. 665–674. DOI: 10.1097/00004728-198010000-00017.

9. Helfen L., Baumbach T., Mikulík P., Kiel D., Pernot P., Cloetens P., Baruchel J. High-resolution three-dimensional imaging of flat objects by synchrotron-radiation computed laminography. *Applied Physics Letters*, 2005, vol. 86, p. 071915. DOI: 10.1063/1.1854735.

10. Grant D.G. Tomosynthesis: a three-dimensional radiographic imaging technique. *IEEE Transactions on Biomedical Engineering*, 1972, vol. BME-19, pp. 20–28. DOI: 10.1109/TBME.1972.324154.

11. Lauritsch G., Härer W.H. Theoretical framework for filtered back projection in tomosynthesis. *Proceedings of SPIE*, 1998, vol. 3338, pp. 1127–1137. DOI: 10.1117/12.310839.

12. Helfen L., Morgeneyer T.F., Xu F., Mavrogordato M.N., Sinclair I., Schillinger B., Baumbach T. Synchrotron and neutron laminography for three-dimensional imaging of devices and flat material specimens. *International Journal of Materials Research*, 2012, vol. 103, pp. 170–173. DOI: 10.3139/146.110668.

13. Fisher S.L., Holmes D.J., Jørgensen J.S., Gajjar P., Behnsen J., Lionheart W.R.B., Withers P.J. Laminography in the lab: imaging planar objects using a conventional x-ray CT scanner. *Measurement Science and Technology*, 2019, vol. 30, p. 035401. DOI: 10.1088/1361-6501/aafcae.

14. Cloetens P., Ludwig W., Baruchel J., Van Dyck D., Van Landuyt J., Guigay J.P, Schlenker M. Holotomography: Quantitative phase tomography with micrometer resolution using hard synchrotron radiation x rays. *Applied Physics Letters*, 1999, vol. 75, pp. 2912–2914. DOI: 10.1063/1.125225.

15. Helfen L., Xu F., Suhonen H., Urbanelli L., Cloetens P., Baumbach T. Nano-laminography for three-dimensional high-resolution imaging of flat specimens. *Journal of Instrumentation,* 2016, vol. 8. DOI: 10.1088/1748-0221/8/05/C05006.

16. Zuber M., Laaß M., Hamann E., Kretschmer S., Hauschke N., Van de Kamp Th., Baumbach T., Koenig T. Augmented laminography, a correlative 3D imaging method for revealing the inner structure of compressed fossils. *Scientific Reports*, 2017, vol. 7. DOI: 10.1038/srep41413**.**

17. Kak A.C., Slaney M. Principles of computerized tomographic imaging. Philadelphia, *Society of Industrial and Applied Mathematics*, 2001. 327 p. DOI: 10.1137/1.9780898719277.

18. Krug K., Porra L., Coan P., Wallert A., Dik J., Coerdt A., Bravin A., Elyyan M., Reischig P., Helfen L., Baumbach T. Relics in medieval altarpieces? Combining X-ray tomographic, laminographic and phase-contrast imaging to visualize thin organic objects in paintings. *Journal of Synchrotron Radiation*, 2008, vol. 15, pp. 55–61. DOI: 10.1107/S0909049507045438.

19. Dik J., Reischig P., Krug K., Wallert A., Coerdt A., Helfen L., Baumbach T. Three-dimensional imaging of paint layers and paint substructures with synchrotron radiation computed μ-laminography. *Journal of the American Institute for Conservation*, 2009, vol. 48, pp. 185–197. DOI: 10.1179/019713612804514260.

20. Houssaye A., Xu F., Helfen L., Buffrénil V.D., Baumbach T., Tafforeau P., Vertebr J. Three-dimensional pelvis and limb anatomy of the Cenomanian hind-limbed snake Eupodophis descouensi (Squamata, Ophidia) revealed by synchrotron-radiation computed laminography. *Journal of Vertebrate Paleontology,* 2011, vol. 31, pp. 2–7. DOI: 10.1080/02724634.2011.539650.

21. Moffat A.J., Wright P., Helfen L., Baumbach T., Johnson G., Spearing S.M., Sinclair I. In situ synchrotron computed laminography of damage in carbon fibre–epoxy $[90/0]_s$ laminates. *Scripta Materialia*, 2010, vol. 62, pp. 97–100. DOI: 10.1016/j.scriptamat.2009.09.027.

22. Castro J., Sket F., Helfen L., Gonzalez C. In situ local imaging and analysis of impregnation during liquid moulding of composite materials using synchrotron radiation computed laminography. *Composites Science and Technology*, 2021, vol. 215. DOI: 10.1016/j.compscitech.2021.108999.

23. Ueda T., Helfen L., Morgeneyer T.F. In situ laminography study of three-dimensional individual void shape evolution at crack initiation and comparison with Gurson–Tvergaard–Needleman-type simulations. *Acta Materialia*, 2014, vol. 78, pp. 254–270. DOI: 10.1016/j.actamat.2014.06.029.

24. Morgeneyer T.F., Taillandier-Thomas T., Helfen L., Baumbach T., Sinclair I., Roux S., Hild F. In situ 3-D observation of early strain localization during failure of thin Al alloy (2198) sheet. *Acta Materialia*, 2014, vol. 69, pp. 78–91. DOI: 10.1016/j.actamat.2014.01.033.

25. Morgeneyer T.F., Helfen L., Sinclair I., Proudhon H., Xu F., Baumbach T. Ductile crack initiation and propagation assessed via in situ synchrotron radiation-computed laminography. *Scripta Materialia*, 2011, vol. 65, pp. 1010–1013. DOI: 10.1016/j.scriptamat.2011.09.005.

26. Shen Y., Morgeneyer T.F., Garnier J., Allais L., Helfen L., Crépin J. Three-dimensional quantitative in situ study of crack initiation and propagation in AA6061 aluminum alloy sheets via synchrotron laminography and finite-element simulations. *Acta Materialia*, 2013, vol. 61, pp. 2571–2582. DOI: 10.1016/j.actamat.2013.01.035.

27. Morgeneyer T.F., Helfen L., Mubarak H., Hild F. 3D digital volume correlation of synchrotron radiation laminography images of ductile crack initiation: an initial feasibility study. *Experimental Mechanics*, 2012, vol. 53, pp. 543–556. DOI: 10.1007/s11340-012-9660-y.

28. Weitkamp T., Tafforeau P., Boller E., Cloetens P., Valade J.-P., Bernard P., Peyrin F., Ludwig W., Helfen L., Baruchel J. Parallel-beam imaging at the ESRF beamline ID19: current status and plans for the future. *AIP Conference Proceedings*, 2010, vol. 1234. DOI: 10.1063/1.3463345.

29. *T*ancogne-Dejeana T., Roth C.C., Morgeneyer T.F., Helfen L., Mohr D. Ductile damage of AA2024-T3 under shear loading: mechanism analysis through in-situ laminography. *Acta Materialia*, 2021, vol. 205, p. 116556. DOI: 10.1016/j.actamat.2020.116556.

30. Roth C.C., Mohr D. Ductile fracture experiments with locally proportional loading histories. *International Journal of Plasticity*, 2015, vol. 79, pp. 328–354. DOI: 10.1016/j.ijplas.2015.08.004.

31. Helfen L., Myagotin A., Rack A., Pernot P., Mikulík P., Di Michiel M., Baumbach T. Synchrotron-radiation computed laminography for high-resolution three-dimensional imaging of flat devices. *Physica Status Solidi (A)*, 2007, vol. 204, pp. 2760–2765. DOI: 10.1002/pssa.200775676.

32. Myagotin A., Voropaev A., Helfen L., Hänschke D., Baumbach T. Efficient volume reconstruction for parallel-beam computed laminography by filtered backprojection on multi-core clusters. *IEEE Transactions on Image Processing*, 2013, vol. 32, pp. 5348–5361. DOI: 10.1109/TIP.2013.2285600.

33. Ando I., Mugita Y., Hirayama K., Munetoh S., Aramaki M., Jiang F., Tsuji T., Takeuchi A., Uesugi M., Ozaki Y. Elucidation of pore connection mechanism during ductile fracture of sintered pure iron by applying persistent homology to 4D images of pores: role of open pore. *Materials Science and Engineering A*, 2021, vol. 828, p. 142112. DOI: 10.1016/j.msea.2021.142112.

34. Hoshino M., Uesugi K., Takeuchi A., Suzuki Y., Yagi N. Development of an x-ray micro-laminography system at Spring-8. *AIP Conference Proceedings*, 2011, vol. 1365, pp. 250–253. DOI: 10.1063/1.3625351.

35. Obayashi I. Volume-optimal cycle: tightest representative cycle of a generator in persistent homology. *SIAM Journal on Applied Algebra and Geometry*, 2018, vol. 2, pp. 508–534. DOI: 10.1137/17M1159439.

36. Kondori B., Morgeneyer T.F., Helfen L., Benzerga A.A. Void growth and coalescence in a magnesium alloy studied by synchrotron radiation laminography. *Acta Materialia*, 2018, vol. 155, pp. 80–94. DOI: 10.1016/j.actamat.2018.05.026.

37. Kondori B., Benzerga A.A. Effect of stress triaxiality on the flow and fracture of Mg alloy AZ31. *Metallurgical and Materials Transactions A,* 2014, vol. 45, pp. 3292–3307. DOI: 10.1007/s11661-014-2211-7.

38. Sano Y., Masaki K., Akita K., Kajiwara K., Sano T. Effect of laser peening on the mechanical properties of aluminum alloys probed by synchrotron radiation and x-ray free electron laser. *Metals*, 2020, vol. 10, p. 1490. DOI: 10.3390/met10111490.

39. Nakai Y., Shiozawaa D., Kikuchia S., Obamaa T., Saitoa H., Makinob T., Neishi Y. Effects of inclusion size and orientation on rolling contact fatigue crack initiation observed by laminography using ultra-bright synchrotron radiation. *Procedia Structural Integrity*, 2016, vol. 2, pp. 3117–3124. DOI: 10.1016/j.prostr.2016.06.389.

40. Shiozawa D., Makino T., Neishi Y., Nakai Y. Observation of rolling contact fatigue cracks by laminography using ultra-bright synchrotron radiation. *Procedia Materials Science*, 2014, vol. 3, pp. 159–164. DOI: 10.1016/j.mspro.2014.06.030.

41. Nakai Y., Shiozawa D., Kikuchi S., Obama T., Saito H., Makino T., Neishi Y. 4D observations of rolling contact fatigue processes by laminography using ultra-bright synchrotron radiation. *Engineering Fracture Mechanics*, 2017, vol. 183, pp. 180–189. DOI: 10.1016/j.engfracmech.2017.03.021.

42. Solano-Alvarez W., Peet M.J., Pickering E.J., Jaiswal J., Bevan A., Bhadeshia H.K.D.H. Synchrotron and neural network analysis of the influence of composition and heat treatment on the rolling contact fatigue of hypereutectoid pearlitic steels. *Materials Science and Engineering: A*, 2017, vol. 707, pp. 259–269. DOI: 10.1016/j.msea.2017.09.045.

43. Zhang S.Y., Spiryagin M., Ding H.H., Wu Q., Guo J., Liu Q.Y., Wang W.J. Rail rolling contact fatigue formation and evolution with surface defects. *International Journal of Fatigue*, 2022, vol. 158, p. 106762. DOI: 10.1016/j.ijfatigue.2022.106762.

Conflicts of Interest

The authors declare no conflict of interest.